Biosensors and Bioelectronics 83 (2016) 293–299

Contents lists available at ScienceDirect

Biosensors and Bioelectronics

journal homepage: www.elsevier.com/locate/bios

Short communication

Magnetic immunoassay platform based on the planar frequency mixing magnetic technique

Chang-Beom Kim [a], Eul-Gyoon Lim [a], Sung Woong Shin [a], Hans Joachim Krause [b,*], Hyobong Hong [a,*]

[a] IT Convergence Research Lab., Electronics and Telecommunications Research Institute (ETRI), Daejeon 34129, Republic of Korea
[b] Peter Grünberg Institute (PGI-8), Forschungszentrum Jülich, 52425 Jülich, Germany

ARTICLE INFO

Article history:
Received 15 February 2016
Received in revised form
15 April 2016
Accepted 22 April 2016
Available online 23 April 2016

Keywords:
Biosensor
Magnetic immunoassay
FMMD
Magnetic nanoparticle
Superparamagnetism
2D magnetic imaging

ABSTRACT

We represent the experimental results of our planar-frequency mixing magnetic detection (p-FMMD) technique to obtain 2D superparamagnetic images for magnetic immunoassay purpose. The imaging of magnetic beads is based on the nonlinear magnetic characteristics inherent in superparamagnetic materials. The p-FMMD records the sum-frequency components originating from both a high and a low frequency magnetic field incident on the magnetically nonlinear nanoparticles. In this study, we apply the p-FMMD technique to 2D scanning imaging of superparamagnetic iron oxide nanoparticles (SPIONs) in a microfluidic platform. Our p-FMMD system enables to acquire planar images of SPIONs filled in a microchannel as narrow as 30 μm in width. The minimum detectable amount is $\sim 1.0 \times 10^8$ beads of 100 nm size. The system shows a spatial resolution enabling to distinguish between two distinct channels even 2 mm apart from each other. Our p-FMMD system as a magnetic immunoassaying system has permitted the detection of amyloid beta 42 ($A\beta_{42}$), a promising biomarker of Alzheimer's disease, at the minimum concentration of 23.8 pg/ml. This may enable the identification of the $A\beta_{42}$ levels for the early-stage of Alzheimer's disease with the assistance of the MPI using p-FMMD technique. The results show that the deployment of the p-FMMD can be an alternative to conventional biosensing analytical methods, and can be used as a fast and portable screening method.

1. Introduction

Microfluidics is frequently applied to biosensing when manipulation and analysis of small amounts of biological fluids is conducted in channels with dimensions of less than hundreds of micrometers. The biochip technology has been extensively utilized in various research areas from molecules and cells to organs and medical diagnosis (Dittrich and Manz, 2006; Mazutis et al., 2013; Weigl, 2006). The miniaturized systems have contributed even to the field of chemical reactions with considerable analytic progress (Brivio et al., 2006; Manz, 1990). In many microfluidic systems, the analysis process in biology and medicine is based on fluorescence for sensitive detection by tagging the analytes with fluorescent dye molecules (Ryu et al., 2011). Long-duration experiments require temporally consistent photostability of fluorescent dyes, which is of major importance for generating accurate analysis of targeted biomaterials during experiments (Medintz et al., 2005). However, time-dependent exponential decay of fluorescent dye occurs in many cases, which is caused by irreversible extinction of fluorescent molecules by high energy excitation (Kuwana and Sevick-Muraca, 2002). Quantum dots (Qdots) have recently received attention in a wide range of biological applications to overcome the drawback of conventional fluorescent dyes (Hu et al., 2014). Although Qdots exhibit better photostability and brightness, they also suffer from a blue-shift of their emission under a few minutes of continuous excitation and eventually achieve a photobleached state (Shi et al., 2013). Therefore, tracers that are not affected by excitation sources are preferable for precise analysis because they generate temporally and functionally stable signals and can be regarded as reliable markers.

Magnetic nanoparticles (MNPs) have been widely used in various fields. Among many different types of MNPs, superparamagnetic iron oxide nanoparticles (SPIONs) are especially useful for biological applications because of high coercivity, high magnetic saturation and susceptibility with time-independent characteristics (Reeves and Weaver, 2014). Thus, SPIONs are very practical for a broad range of applications including the detection of specific biological substances, magnetic bio-separation, therapy and targeted drug delivery. Currently, SPIONs also have been

* Corresponding authors.
E-mail addresses: h.-j.krause@fz-juelich.de (H.J. Krause), hb8868@etri.re.kr (H. Hong).

http://dx.doi.org/10.1016/j.bios.2016.04.076
0956-5663/

utilized in medical imaging as image tracers in the relatively new imaging technology called magnetic particle imaging (MPI) (Bauer et al., 2015; Goodwill et al., 2012; Haegele et al., 2012; Hong et al., 2014). MPI is a novel medical imaging method mapping the *in vivo* spatial distribution or local concentration of the MNPs under the appropriate external magnetic fields. Especially, as the SPIONs exhibit nonlinear magnetization characteristics, the MPI technology holds great promise for highly sensitive, and spatially and temporally high-resolution medical imaging (Borgert et al., 2013; Graefe et al., 2015; Panagiotopoulos et al., 2015).

Recently, a new magnetic detection method was developed based on the nonlinear magnetization of superparamagnetic nanoparticles under the magnetic fields generated by two distinct frequencies, called frequency mixing magnetic detection (FMMD) (Krause et al., 2007). When super-paramagnets are exposed to magnetic fields at two distinct frequencies, sum-frequencies representing a linear combination are generated and signalized by lock-in amplification (Krause et al., 2007). The amplified signals are specifically commensurate with the nonlinearity of the magnetization curve of the nanoparticles (Meyer et al., 2007). Based on the FMMD technique, we present a special type of MPI detector for planar samples (p-FMMD). Compared to the existing MPI instrumentation, a sample magnetization is not required for our p-FMMD system because the generated sum-frequency at $f1+2f2$ is maximum at zero static bias field. Therefore, the measurement setup does not need to be bulky in size because of strong magnets. In fact, the dimensions of the measurement head are only 77 mm × 68 mm × 29 mm. The restriction of our system, however, is that only planar samples with a maximum thickness of 2 mm are accessible due to the narrow dimension of measurement slot. The planar sample is scanned by linear translocation within the intermediate space between two measurement heads. A re-construction allowing for thicker samples is possible, but has to be traded in for a loss of spatial resolution. This novel type of scanner allows to obtain images of the distribution of magnetic particles in planar microfluidic biosensing platforms. The results showed the applicability of the p-FMMD technique to a broad range of potential applications such as early diagnosis tool for Alzheimer's disease. In this study, we applied the p-FMMD technique to the quantification of amyloid beta 42, a promising biomarker of Alzheimer's disease, treated on a planar sensing platform as an early diagnosis tool.

2. Materials

2.1. Superparamagnetic nanoparticle and microfluidic platform

In order to study the sensing dimension limits recognizable by the p-FMMD shown in Fig. 1(a), the SPION was purchased from Chemicell (fluidMAG, Germany). The core material is magnetite and the hydrodynamic diameter is about 100 nm. The nanoparticles are dispersed in a storage buffer (ddH_2O, 0.05% sodium azide), having a total weight of volume of 10 μg/μl. In order to consider the effect of the SPION concentration on the measurement resolution of the p-FMMD, 4 different concentrations were prepared for the experiments: 10.0, 5.0, 2.5, and 1.0 μg/μl, diluted with ddH_2O, which correspond to 1.8×10^{10}, 9×10^9, 4.5×10^9, and 1.8×10^9 beads/μl, respectively.

In order to verify the detection limit of a target protein recognizable by the p-FMMD as a magnetic immunoassaying system, amyloid beta 42 ($A\beta_{42}$) was considered as the target protein, which is a promising biomarker of Alzheimer's disease. The $A\beta_{42}$ peptide solutions were diluted to many different concentrations within the ranges from 7.8 pg/ml to 10 ng/ml, as suggested by the manufacturer protocol (Covance, SIG-38956). The primary polyclonal capture antibody was purchased from Invitrogen (44-344, rabbit, USA), and the primary monoclonal biotinylated detection antibody was purchased from Covance (SIG-39144, mouse, USA). The streptavidin-conjugated SPION was purchased from Ocean NanoTech (MHS-50, USA). The core

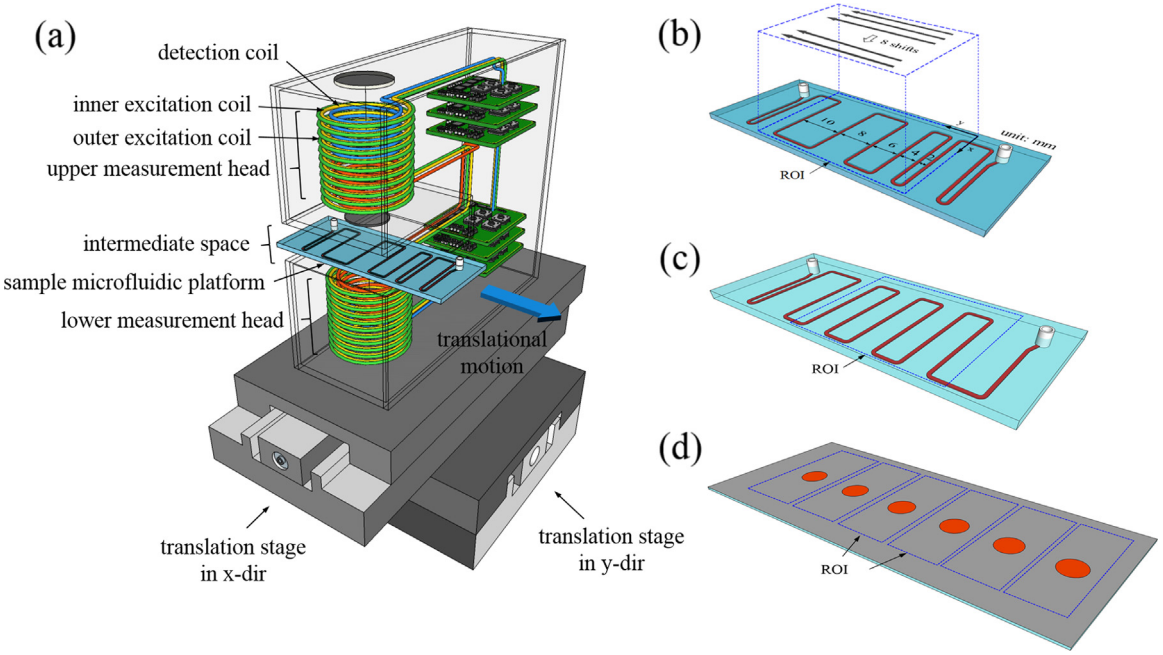

Fig. 1. (a) Schematic diagram of the p-FMMD system composed of the magnetic measurement head and the motorized translation stage. The measurement head is designed in a symmetrical configuration with upper and lower coils, containing a set of two excitation coils and two detection coils in each head. The translation stage is controlled in x and y-direction by an electronic motion controller. (b) A sample microfluidic platform with different widths and intermediate distances. The p-FMMD performs the scanning of the microchannel filled with SPIONs in the range of interest. Arrows indicate the x/y scanning direction during the translational motion of the microfluidic platform. (c) A microchannel with a simple configuration of constant intermediate distance between the adjacent channels. The p-FMMD performs examination of the detection limit for $A\beta_{42}$ peptides. (d) A circular patterned (2 mm in diameter) platform was fabricated for detection of the low concentrations of $A\beta_{42}$ peptides which could not be detected by the microfluidic platforms. (For interpretation of the references to color in this figure, the reader is referred to the web version of this article.)

material is magnetite and the hydrodynamic diameter is about 50 nm. The nanoparticles are pre-blocked with a layer of covalently coupled BSA which may reduce non-specific binding. The total weight of volume is 1.0 μg/μl.

As described in Fig. 1(b), the sample microfluidic platform with a simple microchannel configuration was fabricated using a conventional photolithographic process. A thin microscope cover slip (thickness 170 μm) was used as a substrate due to the narrow intermediate space between the measurement heads. Considering the resolution of the p-FMMD for practical application of MPI to magnetic immunoassay, we need to accurately determine the spatially optimized configuration of the sensing area with recognizable dimensions by the p-FMMD. Therefore, we fabricated the microchannels with different widths ranging from 30 to 300 μm to examine the minimum dimension limit detectable by the p-FMMD under various experimental conditions. The height of all microchannels was kept to be 50 μm. Furthermore, to investigate the scanning resolution regarding discrimination of two adjacent microchannels, the intermediate distance between the neighboring channels varied from 2 to 10 mm along the channel path. The resolution tests were carried out under different conditions in terms of channel width, intermediate distance between neighboring channels, and nanoparticle concentration.

For the magnetic immunoassay, we used to two different platforms: (1) A simple microchannel configuration was used with constant intermediate distance between the adjacent channels (Fig. 1(c)). (2) A circular patterned (2 mm in diameter) platform (Fig. 1(d)) was used for the lower concentrations of $A\beta_{42}$ which could not be detected by the microfluidic platforms. The circular pattern is hydrophobic glass surface and the surrounding is hydrophilic surface treated by paraffin.

2.2. Surface treatment for magnetic immunoassay

Basically, the p-FMMD detects the nonlinear magnetic characteristics of the SPIONs working as tracers for the medical imaging. To examine the detection limit as a magnetic immunoassay, amyloid beta peptide (Sigma-Aldrich) was coated on the sensing platform surface to achieve interaction with the biotinylated antibody. The cover glass was sonicated and washed with ethanol (99.9%, Sigma-Aldrich) for 5 min Then, the oxygen plasma treatment was performed to bind the PDMS microchannel, and to form hydroxyl group on the microchannel and the circular pattern surface, consequently inducing the chemical conjugation between the surface and the capture antibody. The hydroxylated surface was treated by introducing 3-aminopropyl triethoxysilane solution (APTES, 1% in ethanol, Sigma-Aldrich) into the microchannel to form amino functional groups. After incubation for 1 h, the surface was washed with ethanol and baked at 120 °C for 15 min Thereafter, the amine reactive surface was treated with glutaraldehyde solution (GA, 25% in dH_2O, Sigma-Aldrich) containing sodium cyanoborohydride ($NaBH_3CN$, 10 mg/ml in GA solution, Sigma-Aldrich). This process worked as a bifunctional cross-linking to change amino groups to reactive aldehyde groups, which would interact with the capture antibody. After incubation for 4 h, the surface was 3 times washed with dH_2O. The polyclonal capture antibody solution (diluted, 1:300) was introduced to coat the surface at 4 °C for 1 h incubation. Then, a 1 h blocking process was carried out using BSA solution (3% in PBS, Sigma-Aldrich) at 4 °C to block the unreacted surface, which may prevent nonspecific binding of $A\beta_{42}$. After BSA washing with PBS and dH_2O, (1) the $A\beta_{42}$ peptide solutions with 3 different concentrations were introduced into the microchannel: 10, 5, and 1 ng/ml. (2) the $A\beta_{42}$ peptide solutions with 6 different concentrations were introduced onto the circular pattern: 250.0, 138.9, 77.2, 42.9, 23.8, and 13.2 pg/ml. The reaction between $A\beta_{42}$ peptide and capture antibody was incubated overnight at 4 °C. After 3 times washing processes, the monoclonal biotinylated primary detection antibody solution (diluted, 1:300) was introduced on the surface. Followed by the 1 h incubation at 4 °C, the streptavidin-conjugated SPION solution (1.0 μl/μg) was introduced and reacted with biotin during 1 h incubation at 4 °C. The final washing step was performed with special care to prevent the entire removal of the attached nanoparticles due to strong hydraulic pressure. Even though streptavidin and biotin bonding is as strong as a covalent cross-link, the dimension of the nanoparticles is large enough to be affected by the shear flow in the microchannel, and the detachment of the nanoparticles may occur because the bonding may not sustain the hydraulic pressure. Therefore, the applied volume flow rate of the washing solution was about 1.0 μl/s. To minimize nonspecific binding of the streptavidin-conjugated SPIONs, we carried out 3 times washing processes between each step. Finally, we acquired the p-FMMD images of the SPION distribution attached to the surfaces of the microchannel and circular pattern.

3. Methods

3.1. The planar - frequency mixing magnetic detection (p-FMMD) system

As schematically described in Fig. 1(a), the p-FMMD system is mainly composed of two parts: the magnetic measurement head and the motorized translation stage in x and y-direction with a motion controller. The measurement head is designed in a symmetrical configuration with upper and lower coils facing each other. A 2 mm intermediate space in between the two sets of coils allows for the translational motion of a sample microfluidic platform. The magnetic detection unit consists of two measurement heads, one above and one below the microfluidic sample. Each measurement head contains a set of two excitation coils and two detection coils. The excitation coils are wound clockwise (if seen from the top) in both measurement heads. The excitation coils consist of a set of inner (yellow) and outer (green) coils generating a high and a low frequency, respectively. The detection coils are located at the innermost part, and wound clockwise (blue) in half and counter clockwise (red) in another half in each measurement head, as depicted in Fig. 1(a) and functionally explained in (Hong et al., 2014).

The motorized translating stage is controlled by a user-programmed interface using Python. The speed of the stage varies from 0.1 up to 8 mm/s. The spatial traveling range of the stage covers a 25 mm (x-dir) × 60 mm (y-dir) rectangular region at maximum. During the experiments, we adjusted the traveling range to 35 mm translation along the y-axis from the origin, and 8 shifts by 3 mm along the x-axis, corresponding to 21 mm, which constitutes the region of interest (ROI) of the microchannel configuration on the sample platform. The optimized scanning speed for the experiments was set to 0.5 mm/s considering the quality of the output signal. The total scanning time with 0.5 mm/s amounts to about 5 min

3.2. 3D magnetic field simulation

Prior to the experiments, it is important to understand the entire magnetic fields within the intermediate space between the measurement heads. It is also significant to identify the most effective region that receives the maximum excitation fields. The output MPI quality can be significantly enhanced when the microfluidic sample platform translationally moves through the maximum position. Even though the intermediate space is as narrow as 2 mm in height (z-direction), a gradient of the magnetic

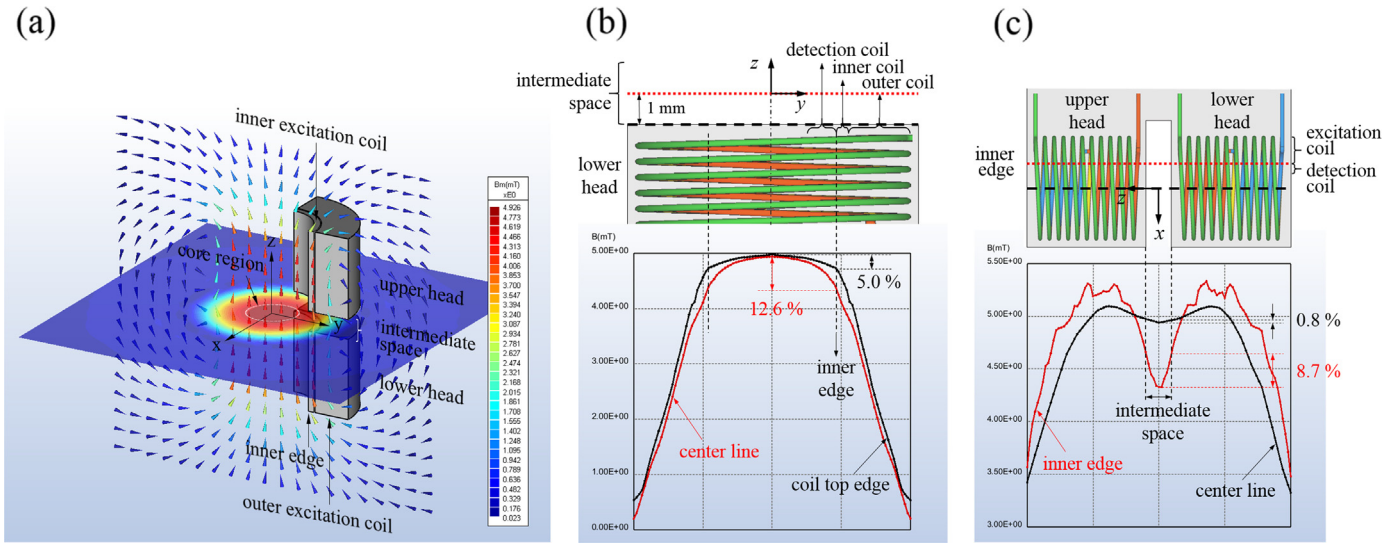

Fig. 2. (a) 3D simulation result of instant magnetic fields generated by magnetic frequency mixing of the fields of the inner and outer excitation coils. The arrow plot shows uniform direction of the fields in the intermediate space, and the contour plot indicates a stable gradient of the fields within the core region of measurement. (b) Horizontal (y-dir) variations of the magnetic strength across the excitation coil. Compared to the center line (·····) in the intermediate space, the top edge of the coil (-----) yields minimum magnetic field gradient (5.0 %), resulting in a more stable environment for measurement. (c) Vertical (z-dir) variations of the magnetic field strength in the intermediate space. The results show that the closer one is to the center line, the smaller the gradients of the magnetic fields are. The magnetic variations along the inner edge (·····) of the excitation coil show maximum magnetic field gradient (8.7 %), while minimum gradient (0.8 %) exists along the z-axis (-----). (For interpretation of the references to color in this figure, the reader is referred to the web version of this article.)

fields induced by the excitation coils will be existent. However, the gradient needs to be minimized within the detection space to establish a stable environment for the imaging measurement. Therefore, a 3D simulation was performed using FARADAY (Integrated Engineering Software, Canada) under the same physical dimensions as the p-FMMD system. Furthermore, information on the magnetic fields inside the coil system can be obtained from the simulation, which may be useful for the design of the entire system.

As seen in Fig. 2(a), the excitation coils were simplified and modeled as circularly swept rectangles covering 90 degrees rotation about the z-axis. By defining angular periodicity, the excitation coil model was reduced only to the single 90-degree angular section, which reduced the total simulation time. The cross section area of the modeled coil was equivalent to the sum of the cross section areas of all individual wires. The input current assigned to the modeled coil volume was equal to the product of the terminal current multiplied by the number of total wire turns. The simulation was performed in AC transient condition with two different frequencies applied to both inner and outer excitation coils. The time harmonic magnetic fields induced by the frequency mixing of the excitation coil fields were successfully obtained, which produce the output signal of the sample microfluidic platform.

4. Results and discussion

4.1. 3D simulation for magnetic fields

Fig. 2(a) shows the model geometry describing the inner and outer excitation coils in a 90-degree angular section out of the entire coil system. The applied boundary conditions were as follows. The terminal currents were 10 mA for the inner coil and 24.5 mA for the outer coil. The input frequencies were 60 Hz for the inner coil and 76,500 Hz for the outer coil. The contour plot designates the magnetic field distribution in the xy-plane at z=0 within the intermediate space. As predicted, the distribution shows a concentric circle about the z-axis, which means symmetrical magnetic fields for any direction. The arrow plot shows the magnitude (in color) and direction of the integrated magnetic field generated from the two different excitation coils, which shows periodical changes according to the frequency mixing (data not shown). This proves that the single 90-degree angular section is properly simplified and modeled. Fig. 2(b) shows the horizontal variations of the magnetic strength calculated across the excitation coil in the y-direction (x=0). The red plot indicates the magnetic field distribution along the y-axis (···). A magnetic field strength of 4.94 mT at the center and 4.32 mT at the innermost edge of the inner excitation coil was obtained, which means that the variation of the magnetic strength is within 12.6%. The gradient of the magnetic fields is slightly steeper in the middle of the intermediate space, which does not seem to be a stable environment for the measurement. The black plot shows the magnetic field distribution on the top surface of the lower head (—). A magnetic strength of 4.98 mT at the center and 4.73 mT at the innermost edge of the inner coil was calculated, which means that the variation of the magnetic field is only within 5.0%. Compared to the center line, the edge of the coil yielded a smaller magnetic field gradient, resulting in a more stable environment for the measurement. Fig. 2(c) shows the vertical variation of the magnetic field strength calculated in the z-direction. The magnetic field is only varying within 0.8% along the z-axis (—) while changing within 8.7% along the inner edge (···). Therefore, the entire magnetic field within the intermediate space was analyzed, and the p-FMMD has been proven to be a stable p-FMMD scanner. Based on the numerical results of the simulation, the optimal region for the sample translational motion was chosen to be immediately above the lower head, not on the center plane in the intermediate space, and within 2 mm in radius from the coil's center, because here the magnetic field gradient becomes minimum in the y-direction on the plane above the coil.

4.2. MPI analysis for sensing dimension limits of the p-FMMD

Fig. 3(a) shows the grayscale-converted images of magnetic particle distribution of 3 microchannels filled with SPIONs of 4 different concentrations, measured using the p-FMMD. As mentioned before, to verify the applicability of the MPI to medical

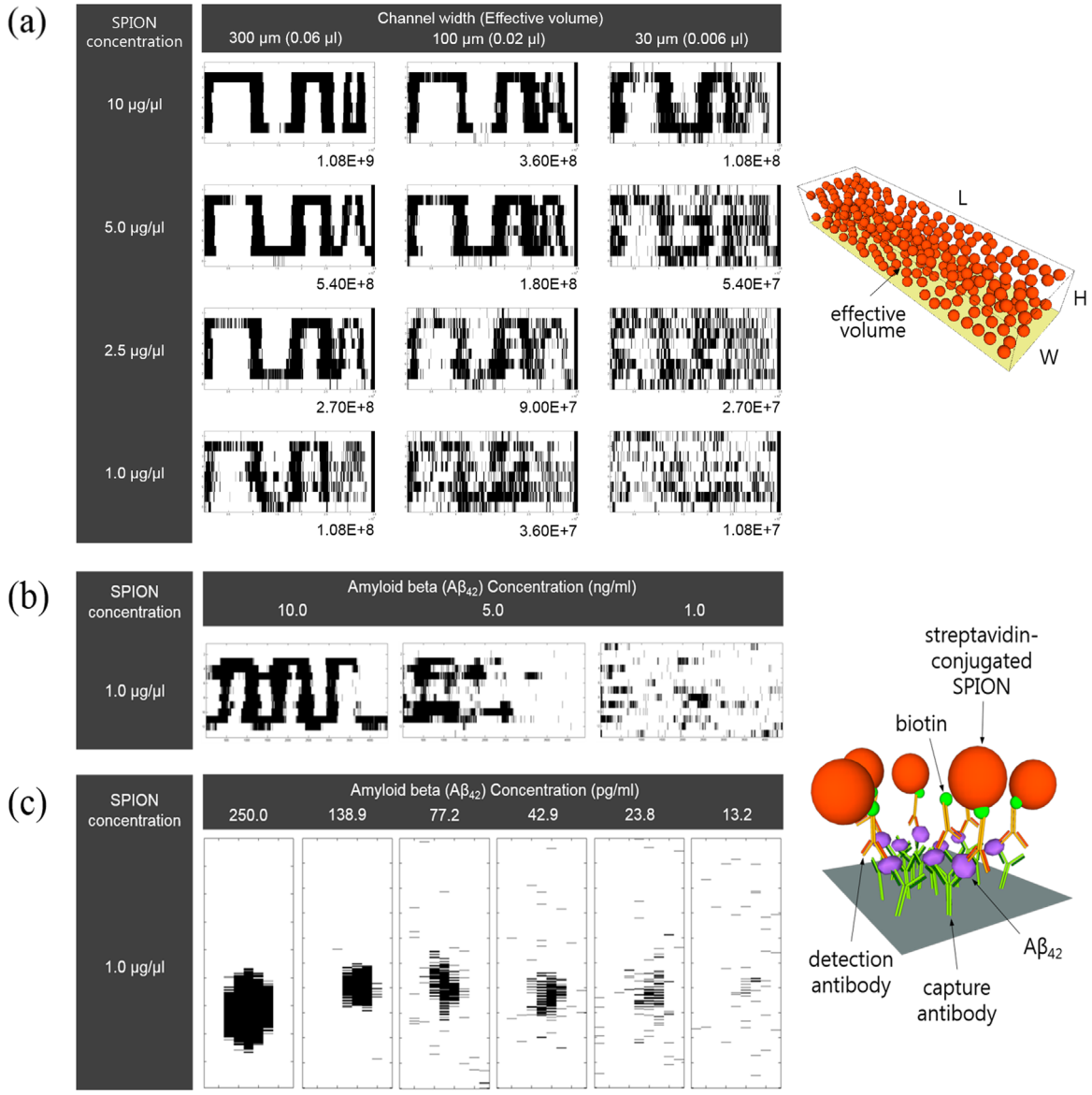

Fig. 3. (a) Magnetic images of the volume-filled SPIONs of different concentrations in different size microchannels. The numbers below each magnetic image indicate the numbers of SPIONs filled in the effective volumes. (b) Magnetic images of the surface-bound SPIONs on the $A\beta_{42}$ attached surface in the microchannels. Amyloid beta 42 ($A\beta_{42}$) peptides in microfluidic platforms were detected clearly at a concentration of 10.0 ng/ml, partly at 5.0 ng/ml, but not recognizable at a concentration of 1.0 ng/ml. (c) Magnetic images of the surface-bound SPIONs on the $A\beta_{42}$ attached surface on the circular patterns. Large reaction sensing areas permitted detection of $A\beta_{42}$ peptides at concentrations as low as 23.8 pg/ml.

imaging diagnostic purposes, we need to examine the sensing dimension limits recognizable by the p-FMMD and quantitatively confirm the optimized spatial configuration. First, to investigate the detection limits of the p-FMMD in terms of the microchannel width, we prepared 3 different channel widths: 30, 100, and 300 μm. As a first step, the highest concentration (10 μg/μl, 1.8×10^{10} beads/μl) of SPION was introduced into the channels, and the p-FMMD images were obtained for all channel widths. Consequently, the p-FMMD was able to clearly recognize all microchannels, even the narrowest one with 30 μm width at the highest concentration. Subsequently, we further decreased the concentration of SPIONs down to 5.0, 2.5, and 1.0 μg/μl and performed scans for each concentration. The p-FMMD performed apparent recognition at a concentration of 5.0 μg/μl, but showed slightly unclear resolution for 30 μm width. The configuration of the channel was recognizable within the background noise. For a concentration of 2.5 μg/μl, the microchannel with 30 μm width was not clearly detectable any more due to the strong background noise while the others showed rather well recognizable features. A similar tendency was observed in the case of 1.0 μg/μl. Therefore, the configurations of the microchannels were clearly recognizable by the p-FMMD at all concentrations, except for the 30 μm wide channels at low concentrations (2.5 and 1.0 μg/μl). The background noise was prominent for channel widths narrower than 30 μm.

For quantitative analysis, we need to consider the number of the SPIONs within an effective channel volume. The MPI images are mainly produced by the SPIONs passing through the core region (within 4 mm in diameter, shown in Fig. 2(a)) of the excitation coils during scanning. The effective volume was defined as the spatial domain (4 mm in length × width × height) effectively influenced by the strong excitation fields while the sample platform traverses the intermediate space during the translational movement, as described in Fig. 3(a). The height of all microchannel was 50 μm, and the widths varied from 30 to 300 μm. With this

approximation, the dimensions of the effective volumes were calculated, and the numbers of the SPION were estimated based on the weight of volume of the undiluted SPION. The p-FMMD clearly recognized microchannels filled with more than $\sim 1.0 \times 10^8$ beads for 300 μm width, $\sim 9.0 \times 10^7$ for 100 μm width, and $\sim 5.0 \times 10^7$ for 30 μm width.

4.3. MPI analysis for discriminatory scanning limits of the p-FMMD

Further analysis was performed by investigating the scanning resolution limit of the p-FMMD in discriminating two adjacent microchannels. As mentioned above, the intermediate distance between the neighboring channels changed from 2 to 10 mm with 2 mm gradation along the channel path, shown in Fig. 1(b). The p-FMMD scanner was able to differentiate all the two neighboring channels at a concentration of 10 μg/μl, even those 2 mm apart. For 5.0 μg/μl, it was not possible to clearly discriminate the channels less than 4 mm apart for 30 μm width, but the others were distinctly observable. For 2.5 μg/μl, the p-FMMD scanner was not able to image the 30 μm wide channels at all, but worked for the others. For the lowest concentration, the p-FMMD scanner was able to partly distinguish two channels, but did not work for the rest.

The p-FMMD can apparently recognize most of the adjacent microchannels with the intermediate distances from 2 to 10 mm for the microchannels wider than 100 μm. This is due to the fact that a minimum number of SPIONs is needed within the sensitive volume in order to obtain sufficiently strong signals which are distinguishable from the noise floor. In other words, there exists a minimum amount of SPIONs generating nonlinear frequency mixing signal high enough to overcome the noisy background signals.

4.4. Detection limit experiment for magnetic immunoassay using p-FMMD

Fig. 3(b) shows the grayscale magnetic images of the 3 microchannels with the surface attachment of $A\beta_{42}$ peptide at higher concentrations than 1.0 ng/ml. The streptavidin-conjugated SPIONs (50 nm in diameter) at a concentration of 1.0 μg/μl were introduced into the microchannel, and were attached to the biotinylated-ends of the $A\beta_{42}$ monoclonal detection antibody. We obtained magnetic images of the 2-dim surface-bound magnetic particles, which would verify the p-FMMD performance as a magnetic immunoassay system. For the $A\beta_{42}$ concentrations of 5.0 and 10.0 ng/ml, the microchannels was partly and entirely recognizable by the p-FMMD, respectively. However, the p-FMMD system was not able to clearly detect the SPIONs at a concentration of 1.0 ng/ml. Concentration of 1.0 ng/ml is not considered to be a low concentration for a classical immunoassay. A possible reason could be the fact that the actual binding efficiency of the streptavidin-conjugated SPION onto the biotinylated antibody treated surface is lower than estimated. Assuming that the streptavidin-conjugated SPIONs could completely fill the effective surface (the xy-surface in the effective volume) without any empty space, the maximum number of the surface-bound SPION were estimated to be $\sim 6.1 \times 10^8$ for 300 μm width microchannel. In addition, the p-FMMD signals of surface-bound SPIONs may be lower than those of particles swimming freely in the liquid because the Brownian relaxation is inhibited in case of the bound particles. Therefore, the performance of the current p-FMMD system with microchannel is capable of generating magnetic images for $A\beta_{42}$ concentrations of higher than 1.0 ng/ml.

For verification of the potential of the p-FMMD to detect $A\beta_{42}$ concentrations less than 1.0 ng/ml, we prepared circular patterned platforms with 2 mm diameter. This sensing area increases 2.6 times bigger than the effective surface of the microchannel. The circular pattern was treated to be hydrophilic while the surrounding to be hydrophobic. Fig. 3(c) shows the grayscale magnetic images of the circular patterned platforms. Six different concentrations of $A\beta_{42}$ were prepared according to a manufacturer protocol. The concentrations varied from 250 pg/ml down to 13.2 pg/ml at the minimum. The p-FMMD was able to recognize up to 23.8 pg/ml of $A\beta_{42}$ even though the signal intensity was very low. Compared to the detection limit ($\sim$ 7 pg/ml) of a commercial ELISA kit, our system showed a high performance for identification of $A\beta_{42}$ peptides. This method demonstrates a facile approach for the analysis of $A\beta_{42}$ quantification using MPI technique and SPIONs.

5. Conclusions

To verify the applicability of the MPI of our p-FMMD system to medical imaging diagnostic purposes, we examined the sensing dimension limits recognizable by the system and quantitatively confirm the optimized spatial configuration. We acquired p-FMMD images of volume-filled SPIONs in microchannel as narrow as 30 μm as a detectable dimension limit, and the system enabled to distinguish two distinct channels 2 mm apart from each other as a spatial resolution. To properly work at the both limits, the p-FMMD system requires at least $\sim 1.0 \times 10^8$ of SPIONs at the minimum. This is due to the fact that a minimum number of SPIONs is needed within the sensitive volume in order to obtain sufficiently strong signals which are distinguishable from the noise floor. There should be a minimum amount of SPIONs generating nonlinear frequency mixing signal high enough to overcome the noisy background signals.

And, we demonstrated the feasibility of the p-FMMD for magnetic immunoassay as it precisely detected surface-bound SPION tracers at a level as low as 23.8 pg/ml of $A\beta_{42}$ peptides. It might be slightly higher than commercial ELISA systems. In this study, we used a planar sensing platform that enables the identification of the $A\beta_{42}$ levels for the early-stage of Alzheimer's disease with the assistance of MPI technique. According to current medical paradigmatic transition from medical treatment to early diagnostic prevention, a simple sensing platform has been considered as an important tool by which the promising AD biomarkers could be verified. Our measuring method did not require complicated, time-consuming, and labor-dependent processes, and high-end devices. Therefore, it is expected that our p-FMMD system is applicable as a 2-dimensional diagnostic system for magnetic immunoassay biochip with MPI technique.

Acknowledgments

This work was supported by Institute for Information & communications Technology Promotion (IITP) grant funded by the Korea government (MSIP) (No. B132-15-1001).

Appendix A. Supporting information

Supplementary data associated with this article can be found in the online version at http://dx.doi.org/10.1016/j.bios.2016.04.076.

References

Bauer, L.M., Situ, S.F., Griswold, M.A., Samia, A.C., 2015. J. Phys. Chem. Lett. 6 (13), 2509–2517.
Borgert, J., Schmidt, J.D., Schmale, I., Bontus, C., Gleich, B., David, B., Weizenecker, J.,

Jockram, H., Lauruschkat, C., Mende, O., Heinrich, M., Halkola, A., Bergmann, J., Woywode, O., Rahmer, J., 2013. Biomed. Tech. Biomed. Eng. 58 (6), 551–556.
Brivio, M., Verboom, W., Reinhoudt, D.N., 2006. Lab Chip 6, 329–344.
Dittrich, P.S., Manz, A., 2006. Nat. Rev. Drug. Discov. 5, 210–218.
Goodwill, P.W., Lu, K., Zheng, B., Conolly, S.M., 2012. Rev. Sci. Instrum. 83 (3), 033708.
K., Graefe, A., von Gladiss, G., Bringout, M., Ahlborg, T., Buzug, 2015. IEEE Transactions on Medical Imaging.
Haegele, J., Sattel, T., Erbe, M., Luedtke-Buzug, K., Taupitz, M., Borgert, J., Buzug, T.M., Barkhausen, J., Vogt, F.M., 2012. RoFo: Fortschritte Gebiete Rontgenstrahlen Nuklearmed. 184 (5), 420–426.
Hong, H., Lim, J., Choi, C.J., Shin, S.W., Krause, H.J., 2014. Rev. Sci. Instrum. 85 (1), 013705.
Hu, S., Zeng, S., Zhang, B., Yang, C., Song, P., Hang Danny, T.J., Lin, G., Wang, Y., Anderson, T., Coquet, P., Liu, L., Zhang, X., Yong, K.-T., 2014. Analyst 139 (18), 4681–4690.
Krause, H.-J., Wolters, N., Zhang, Y., Offenhäusser, A., Miethe, P., Meyer, M.H.F., Hartmann, M., Keusgen, M., 2007. J. Magn. Magn. Mater. 311 (1), 436–444.
Kuwana, E., Sevick-Muraca, E.M., 2002. Biophys. J. 83 (2), 1165–1176.
Manz, A., 1990. Sens. Actuators B 1, 244–248.
Mazutis, L., Gilbert, J., Ung, W.L., Weitz, D.A., Griffiths, A.D., Heyman, J.A., 2013. Nat. Protoc. 8 (5), 870–891.
Medintz, I.L., Uyeda, H.T., Goldman, E.R., Mattoussi, H., 2005. Nat. Mater. 4 (6), 435–446.
Meyer, M.H.F., Krause, H.-J., Hartmann, M., Miethe, P., Oster, J., Keusgen, M., 2007. J. Magn. Magn. Mater. 311 (1), 259–263.
Panagiotopoulos, N., Duschka, R.L., Ahlborg, M., Bringout, G., Debbeler, C., Graeser, M., Kaethner, C., Ludtke-Buzug, K., Medimagh, H., Stelzner, J., Buzug, T.M., Barkhausen, J., Vogt, F.M., Haegele, J., 2015. Int. J. Nanomed. 10, 3097–3114.
Reeves, D.B., Weaver, J.B., 2014. Crit. Rev. Biomed. Eng. 42 (1), 85–93.
Ryu, G., Huang, J., Hofmann, O., Walshe, C.A., Sze, J.Y.Y., McClean, G.D., Mosley, A., Rattle, S.J., deMello, J.C., deMello, A.J., Bradley, D.D.C., 2011. Lab Chip 11 (9), 1664–1670.
Shi, X., Tu, Y., Liu, X., Yeung, E.S., Gai, H., 2013. Phys. Chem. Chem. Phys. 15 (9), 3130–3132.
Weigl, B., 2006. Proc. SPIE 6112, pp. 1–11.